

## Conjugates of Heme-Thiolate Enzymes with Photoactive Metal-Diimine Wires

Stephen M. Contakes<sup>1</sup> · Yen Hoang Le Nguyen<sup>1</sup> · Harry B. Gray<sup>1</sup> (✉) · Edith C. Glazer<sup>2</sup> · Anna-Maria Hays<sup>3</sup> · David B. Goodin<sup>2</sup>

<sup>1</sup>Beckman Institute, California Institute of Technology, 1200 E. California Blvd., Pasadena, CA 91125, USA  
*hbgray@caltech.edu*

<sup>2</sup>Department of Molecular Biology, The Scripps Research Institute, 10550 N. Torrey Pines Rd., La Jolla, CA 92037, USA

<sup>3</sup>AMBRX, 10975 N. Torrey Pines Rd., La Jolla, CA 92037, USA

1	Probing Enzymes with Molecular Wires . . . . .	178
2	Molecular Wires for Cytochromes P450 . . . . .	180
2.1	Binding . . . . .	181
2.2	Probing Open States . . . . .	187
2.3	Sensing . . . . .	193
3	Molecular Wires for Inducible Nitric Oxide Synthase . . . . .	195
3.1	Binding . . . . .	196
3.2	Sensing . . . . .	199
4	Conclusions . . . . .	200
	References . . . . .	201

**Abstract** Heme-thiolate enzymes, notably cytochromes P450 and nitric oxide synthases, use dioxygen to oxygenate substrates. Photoactive metal-diimine molecular wires that are capable of effecting rapid redox state changes at buried active sites have been developed to generate intermediates in the catalytic cycles of these enzymes. Wires that feature a photoactive head group tethered to an active-site ligand bind P450CAM and inducible nitric oxide synthase (iNOS) primarily by hydrophobic interactions. The wire-binding specificity of each enzyme is critically dependent on the structural flexibility of the protein. P450CAM:wire conjugates can adopt open or partially open conformations, thereby accommodating a wide range of wires, whereas only long wires with smaller  $[\text{Re}(\text{CO})_3(\text{bpy})\text{Im}]^+$  head groups are able to bind tightly in the rigid active-site channel of iNOS. Dansyl-terminated molecular wires function as highly sensitive and isoform specific fluorescent sensors for P450CAM.

**Keywords** Molecular Wires · Cytochromes P450 · Nitric Oxide Synthase · Photochemistry · Electron Transfer

### Abbreviations

Ad adamantyl  
BH<sub>4</sub> tetrahydrobiopterin

CPR	cytochrome P450 reductase
EB	ethylbenzene
eNOS	endothelial nitric oxide synthase
ET	electron transfer
FAD	flavin adenosine dinucleotide
FET	fluorescence energy transfer
FMN	flavin mononucleotide
iNOS	inducible nitric oxide synthase
iNOS <sub>oxy</sub>	oxygenase domain of inducible NOS
NADPH	nicotinamide adenosine dinucleotide hydride
NHE	normal hydrogen electrode
nNOS	neuronal nitric oxide synthase
NOS	nitric oxide synthase
P450	cytochrome P450
P450BM3	cytochrome P450 from <i>Bacillus megaterium</i>
P450CAM	cytochrome P450 from <i>Pseudomonas putida</i>
pdx	putidaredoxin
tm	tetramethyl

## 1

### Probing Enzymes with Molecular Wires

The definitive characterization of catalytically relevant metalloenzyme redox states is a major challenge in bioinorganic chemistry research, as many redox-active intermediates are formed after the rate-determining steps in catalytic cycles. High-valent compound I and II ferryl species, such as those postulated to effect substrate oxidation in cytochrome P450 and nitric oxide synthase (NOS) reaction cycles, are particularly prominent examples. Both P450 and NOS employ a cysteine-coordinated heme oxygenase domain to activate oxygen through multiple electron transfer (ET) processes: in class I P450CAM systems, a terminal oxygenase domain receives its electrons from NADPH via a FAD containing cytochrome P450 reductase (CPR) domain; in class II drug metabolizing P450 [1, 2] systems, the NADPH reducing equivalents are delivered to an unusual diflavin (FAD and FMN) containing CPR module fused onto its oxygenase domain [3, 4]. NOS isoforms employ fused diflavin containing domains similar to those of the class II P450s [4].

Although ferryl intermediates of horseradish peroxidase and microperoxidase-8 have been produced in reactions with photogenerated  $[\text{Ru}(\text{bpy})_3]^{3+}$  [5], analogous experiments with P450s were unsuccessful, presumably due to the inefficiency of electron transfer from the buried heme active site through the protein backbone [6]. Photoactive molecular wires (sometimes referred to as metal-diimine wires, sensitizer-tethered substrates, or electron tunneling wires) were developed to circumvent this problem by providing a direct ET pathway between  $[\text{Ru}(\text{bpy})_3]^{3+}$  and the heme. These molecular wires, which combine the excellent photophysical properties of metal-diimine complexes

with the facile electron tunneling properties of molecular chains, can be used to generate reactive redox states associated with buried enzyme active sites: a case in point is work in which we successfully generated several novel cytochrome P450 redox states using flash-quench methods [6]. Our investigations also have revealed key factors that contribute to the binding of molecular wires to several different metalloenzymes, including cytochrome P450CAM [7–11], inducible nitric oxide synthase [12, 13], *Arthrobacter globiformis* amine oxidase [14, 15], myeloperoxidase [16], and lipoxygenase [17]; and crystallographic analyses of enzyme:wire conjugates have shed light on conformational changes associated with substrate binding and product egress [7–9]. Importantly, we have demonstrated that molecular wires can function as enzyme inhibitors [15], fluorescent sensors [10, 11], and electrochemical sensors [14].

Molecular wires consist of a ligand with affinity for a buried active site tethered to a head group that binds at the active-site channel surface (Fig. 1). The head group is optimized for the desired functionality: electron tunneling wires employ  $\text{Ru}^{\text{II}}$  or  $\text{Re}^{\text{I}}$  diimine complexes; certain other fluorescent sensors use dyes such as dansyl [10, 11] or fluorescein [16], and electrochemical wire sensors contain thiol or pyrene groups that can be attached to electrode surfaces [14]. The tether, which connects the ligand and head group and resides in the substrate access channel, provides an electron tunneling pathway for injection or abstraction of electrons to and from the active site. The head group, tether, and ligand can be optimized to bind the enzyme of interest. In favorable cases, studies of enzyme:wire complexes reveal the factors that govern substrate specificity for a given enzyme.

We turn our attention now to cytochromes P450 and inducible nitric oxide synthase, where certain key features of wire:protein interactions have been elucidated.

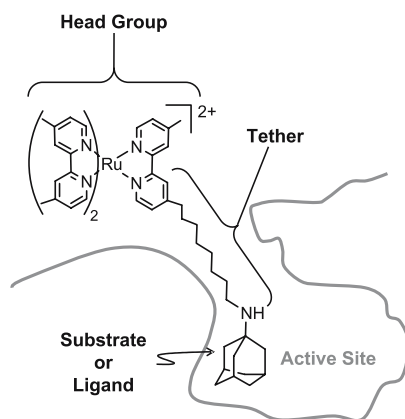


**Fig. 1** Electron tunneling wires consist of a substrate or ligand tethered to a redox-active head group

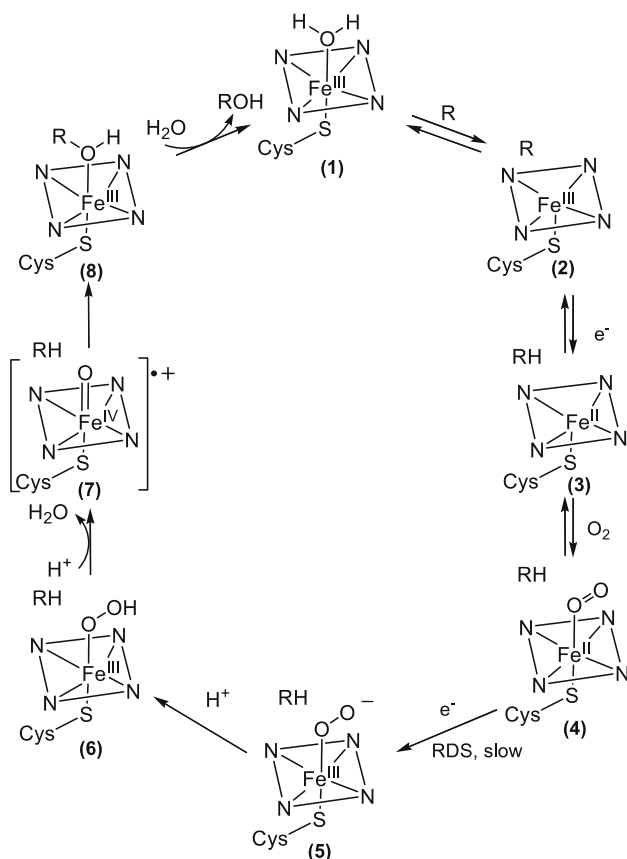
## 2 Molecular Wires for Cytochromes P450

The heme-thiolate cytochromes P450 (P450) catalyze regio- and stereospecific reactions under physiological conditions [18–20], including the hydroxylation of hydrocarbons (Equation Eq. 1), alkene epoxidation, heteroatom (N,S) oxidation, dealkylation, and (anaerobic) dehalogenation [21].



*In vivo* activities include hormone biosynthesis, xenobiotic elimination, drug (de-)activation, and carcinogenesis [22], while potential *in vitro* applications range from chemical synthesis [23] to biosensing [24].

Central to P450 catalysis is electron transfer. The catalytic cycle (Scheme 1) involves two one-electron reductions: catalysis is initiated with the first, while



**Scheme 1** P450 catalytic cycle

the overall rate is limited by the second. Much effort has been expended to investigate the factors that govern ET to and from P450 heme centers in order to understand the catalytic mechanism and ultimately harness P450 oxidation chemistry for *in vitro* applications. The ability to access and characterize compound I is central to the understanding of P450 function. While several heroic attempts have been made to observe such high-valent species in the catalytic cycle [25–28], none has led to definitive characterization of compound I.

We developed molecular wires with the goal of generating P450-I and II by direct photooxidation of the P450 heme. Although our work with electron tunneling wires has demonstrated the feasibility of photochemically inducing P450 redox reactions, definitive characterization of catalytically relevant intermediates has yet to be realized [29]. Nevertheless, our work has illuminated several features of P450 catalysis. P450 wire binding profiles illustrate the factors that govern substrate binding in the active site and its channel. Crystallographic studies of P450:wire complexes reveal novel open conformations that provide insight into the role of low-lying conformational states in P450's ability to oxygenate a wide range of substrates under conditions that require exclusion of water from the active-site channel. Wires also have been developed for use as highly selective isoform-specific fluorescent sensors for P450CAM.

## 2.1 Binding

The molecular wires developed for use with P450 isoforms are shown in Fig. 2. The structures, binding affinities, and ET properties of P450-wire conjugates vary widely, depending on the nature of the tethers and terminal groups, although all employ neutral or positively charged head groups (Table 1).

All of the molecular wires in Fig. 2 are isoform specific: they reversibly bind P450CAM to form conjugates with micromolar to nanomolar dissociation constants; but they do not bind P450BM3 [30]. This selectivity parallels the substrate profiles of the two enzymes: while P450CAM shows maximal activity with adamantyl-like substrates, P450BM3 prefers long chain fatty acids. P450BM3 has an arginine (Arg<sup>47</sup>) at the mouth of the putative substrate access channel, which has been proposed to stabilize the carboxylate group of bound fatty acid substrates [31]. Since positively charged head groups interact unfavorably with this Arg residue, we have designed wires with negatively charged sensitizers to probe P450BM3 [32].

All of our P450CAM molecular wires bind in the active-site channel, as established by the Ru–Fe heme distances ( $\leq 22.1$  Å) determined by fluorescence energy transfer (FET), crystallographic analyses, and competition experiments with the natural substrate (camphor). Imidazole-terminated

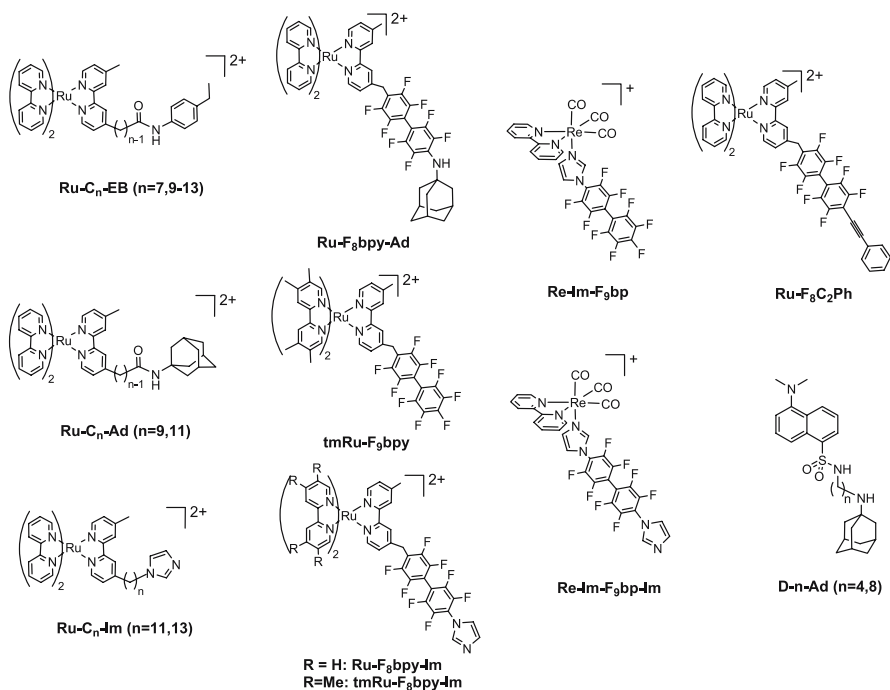


**Fig. 2** Molecular wires that bind cytochrome P450CAM

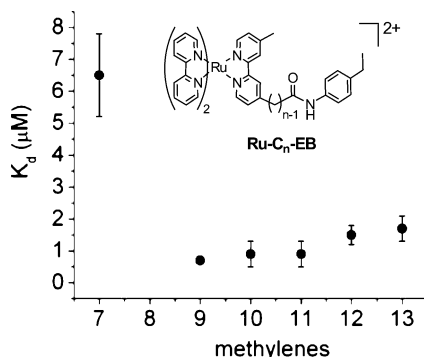


**Fig. 3** Dependence of  $K_d$  on tether length for P450:  $[\text{Ru} - \text{C}_n - \text{EB}]^{2+}$  complexes

metal-diimine wires directly ligate the heme Fe, as evidenced by a shift in the Soret peak from 416 to 420 nm [6, 33]. Notably, the spectral shift indicates that water is not fully displaced from the active site [34–36], a result that differs from the complete heme ligation observed with imidazole, suggesting that there is greater accessibility of water to the heme in the open

**Table 1** P450CAM-wire conjugates

Wire <sup>a</sup>	$K_d$ ( $\mu\text{M}$ )	$d_{\text{M-Fe}}$ ( $\text{\AA}$ )	Comments <sup>b</sup>	Refs.
[Ru - F <sub>8</sub> bpy - Ad] <sup>2+</sup>	0.077 ± 0.001 <sup>f</sup>	22.1 <sup>b</sup> 21.8 <sup>c</sup>	d	[8, 33]
[tmRu - F <sub>9</sub> bpy] <sup>2+</sup>	2.1 ± 0.5 <sup>f</sup>	17.0 <sup>b</sup>	d	[33]
[Ru - F <sub>8</sub> bpy - Im] <sup>2+</sup>	3.7 ± 0.5 <sup>f</sup>	18.1 <sup>b</sup>	Direct photoreduction 30% Fe <sup>II</sup> produced $k_f = 4.4 \times 10^6 \text{ s}^{-1}$ ; $k_b \sim$ undetermined	[33]
[tmRu - F <sub>8</sub> bpy - Im] <sup>2+</sup>	0.48 ± 0.18 <sup>f</sup>	18.1 <sup>b</sup>	Direct photoreduction 74% Fe <sup>II</sup> produced $k_f = 2.8 \times 10^7 \text{ s}^{-1}$ ; $k_b \sim 1.7 \times 10^8 \text{ s}^{-1}$	[33]
[Ru - C <sub>11</sub> - Im] <sup>2+</sup>	> 50 <sup>f</sup>		e	[11, 35]
[Ru - C <sub>13</sub> - Im] <sup>2+</sup>	4.1 <sup>f</sup>	21.2 <sup>b</sup>	d	[6, 11, 35]
[Ru - C <sub>9</sub> - Ad] <sup>2+</sup>	0.4 <sup>f</sup> 0.24 ± 0.2 <sup>g</sup> 0.09( $\Delta$ ) <sup>g</sup> , 0.19( $\Delta$ ) <sup>g</sup> 0.20 ± 0.5( $\Delta$ ) <sup>h</sup> 0.30 ± 0.5( $\Delta$ ) <sup>h</sup>	21.4 <sup>b</sup>	ET after reductive quench $k_f = 2 \times 10^4 \text{ s}^{-1}$ e	[11, 35, 39]
[Ru - C <sub>11</sub> - Ad] <sup>2+</sup>	0.6 <sup>f</sup>	21.0 <sup>b</sup>	d	[6, 11, 35, 39]
			ET after reductive quench with <i>p</i> -MDMA yields [P <sub>Cys</sub> - Fe <sup>II</sup> (H <sub>2</sub> O)] <sup>-</sup> $k_f = 2 \times 10^4 \text{ s}^{-1}$	

Table 1 continued

Wire <sup>a</sup>	$K_d$ ( $\mu\text{M}$ )	$d_{\text{M-Fe}}$ ( $\text{\AA}$ )	Comments <sup>b</sup>	Refs.
[Ru - C <sub>7</sub> - EB] <sup>2+</sup>	6.5 <sup>f</sup>	19.5 <sup>b</sup>	d ET after reductive quench with <i>p</i> -MDMA yields [P <sub>Cys</sub> - Fe <sup>II</sup> (H <sub>2</sub> O)] <sup>-</sup> $k_f \sim 10^3 \text{ s}^{-1}$	[11, 35]
[Ru - C <sub>9</sub> - EB] <sup>2+</sup>	0.7 <sup>f</sup>	19.4 <sup>b</sup>	d ET after reductive quench with <i>p</i> -MDMA yields [P <sub>Cys</sub> - Fe <sup>II</sup> (H <sub>2</sub> O)] <sup>-</sup>	[11, 35]
[Ru - C <sub>10</sub> - EB] <sup>2+</sup>	0.9 <sup>f</sup>	19.9 <sup>b</sup>	d ET after reductive quench with <i>p</i> -MDMA yields [P <sub>Cys</sub> - Fe <sup>II</sup> (H <sub>2</sub> O)] <sup>-</sup>	[11, 35]
[Ru - C <sub>11</sub> - EB] <sup>2+</sup>	0.9 <sup>f</sup>	20.1 <sup>b</sup>	d ET after reductive quench with <i>p</i> -MDMA yields [P <sub>Cys</sub> - Fe <sup>II</sup> (H <sub>2</sub> O)] <sup>-</sup> $k_f = 2 \times 10^4 \text{ s}^{-1}$	[6, 11, 35]
[Ru - C <sub>12</sub> - EB] <sup>2+</sup>	1.5 <sup>f</sup>	20.5 <sup>b</sup>	d ET after oxidative quench with [Co(NH <sub>3</sub> ) <sub>5</sub> Cl] <sup>2+</sup> gives [P <sub>Cys</sub> - Fe <sup>IV</sup> (HO)]? or a porphyrin radical $k_f = 6 \times 10^3 \text{ s}^{-1}$	[11, 35]
[Ru - C <sub>13</sub> - EB] <sup>2+</sup>	1.7 <sup>f</sup>	20.6 <sup>b</sup>	d ET after reductive quench with <i>p</i> -MDMA yields [P <sub>Cys</sub> - Fe <sup>II</sup> (H <sub>2</sub> O)] <sup>-</sup>	[11, 35]
[Re - Im - F <sub>8</sub> bp - Im] <sup>+</sup>	0.6 ± 0.5		d ET after reductive quench with <i>p</i> -MDMA yields [P <sub>Cys</sub> - Fe <sup>II</sup> (H <sub>2</sub> O)] <sup>-</sup>	[36]

**Table 1** continued

Wire <sup>a</sup>	$K_d$ ( $\mu\text{M}$ )	$d_{\text{M-Fe}}$ ( $\text{\AA}$ )	Comments <sup>b</sup>	Refs.
[Re - Im - F <sub>9</sub> bp] <sup>+</sup>	22 ± 8		d	[36]
[Ru - F <sub>8</sub> - C <sub>2</sub> Ph]	0.75	23.1 <sup>c</sup>	d	[16]
D - 8 - Ad	~ 0.02 h	N/A	N/A	[9, 10]

<sup>a</sup> See Fig. 11

<sup>b</sup> Distances were determined from time-resolved emission experiments using the Förster relationship

<sup>c</sup> Distance was determined by X-ray crystallography

<sup>d</sup> Direct photoinduced ET was not observed

<sup>e</sup> Photochemical data are not available

<sup>f</sup> Dissociation constants determined by deconvolution of transient emission spectra

<sup>g</sup> Dissociation constants determined by UV-titrations with camphor

<sup>h</sup> Value represents an upper-limit estimate of the dissociation constant

P450:wire complex (Sect. 2.2) [35]. Perhaps not surprisingly, full ligation of the heme can be achieved for ferrous P450, for which water is a poor ligand [35].

Wires terminated by hydrophobic substrates are incapable of coordinating the heme directly. When these wires bind P450CAM, water may or may not be displaced from the active site. Alkyl-tethered wires with ethylbenzene substrates do not produce significant changes in heme ligation or spin state on binding [35], whereas alkyl and perfluorobiphenyl-tethered adamantyl wires cause partial displacement of coordinated water from the active site [34–36].

The dissociation constants for P450CAM:wire complexes depend on the nature of the substrate, tether, and head group (Table 1); they reflect the neutral hydrophobic character of the P450CAM active-site channel. The highest binding constants are observed for wires containing hydrophobic substrates such as adamantyl and ethylbenzene. Interestingly, wires terminated with imidazole groups ligate the heme but bind ca. 4–20 times more weakly; for example,  $[\text{Ru} - \text{F}_9\text{bpy}]^{2+}$  binds more tightly than  $[\text{Ru} - \text{F}_8\text{bpy} - \text{Im}]^{2+}$ , suggesting that the imidazole actually destabilizes the P450:wire complex, consistent with an energetic penalty associated with desolvation of imidazole on binding in the hydrophobic active site [35]. Evidence also indicates that there is greater accessibility of water to the active site in the open P450 conformation of the P450CAM:wire complex [9], as P450CAM displays 100-fold discrimination between 1-phenyl imidazole ( $K_d = 0.4 \mu\text{M}$ ) and 4-phenyl imidazole ( $K_d = 40 \mu\text{M}$ ) [37, 38]. Hydrophobic linker and head groups promote tight binding, as can be seen by the lower dissociation constants in P450:wire complexes containing perfluorobiphenyl linkers and the 10-fold decrease in  $K_d$  observed for  $[\text{tmRu} - \text{F}_8\text{bpy} - \text{Im}]^{2+}$  vs.  $[\text{Ru} - \text{F}_8\text{bpy} - \text{Im}]^{2+}$ . The tether length also is a factor (Fig. 3):  $K_d$  values exhibit a slight tether length dependence in wires where the tether is long enough to permit access of the substrate group to the heme, whereas wires with shorter tethers bind much more weakly or not at all.

The  $\Lambda$  and  $\Delta$  enantiomers of wires with metal tris-chelate head groups interact differently with the chiral P450CAM active-site channel. Experiments with enantiopure  $\Lambda$ - and  $\Delta$ - $[\text{Ru} - \text{C}_9 - \text{Ad}]\text{Cl}_2$  wires indicate that the  $\Lambda$  enantiomer binds  $\sim 1.5$ – $2$  times more tightly even though the Ru–Fe distances are indistinguishable [39]. The small difference in  $K_d$ s for the two enantiomers suggests that hydrophobic interactions with the adamantyl substrate are more important than induced fit of the head group at the mouth of the active-site channel. The slight preferential binding of  $\Lambda$ - $[\text{Ru} - \text{C}_9 - \text{Ad}]\text{Cl}_2$  may be due to more favorable hydrophobic  $\pi$ -stacking interactions between the bpy groups and Phe<sup>193</sup> and Tyr<sup>29</sup>, a proposal consistent with the P450CAM: $[\text{Ru} - \text{C}_9 - \text{Ad}]^{2+}$  crystal structure (Sect. 2.2) [39].

## 2.2 Probing Open States

Crystal structures have been reported for conjugates between P450CAM and  $[\text{Ru} - \text{C}_9 - \text{Ad}]^{2+}$  [11],  $[\text{Ru} - \text{F}_8\text{bpy} - \text{Ad}]^{2+}$  [8], D-4-Ad [9], and D-8-Ad [9, 10]. Several of the P450CAM:wire structures are shown in Fig. 4 along with that of P450CAM: camphor [9, 33]. In the camphor complex (Fig. 4a), P450CAM possesses a native closed structure in which there is no clear path to the buried heme. In the P450:wire conjugates, the adamantyl substrate groups are bound in the active site and occupy similar positions to that observed in the P450:adamantane complex [40]. The tether/head group traces a path to the enzyme surface and forces P450CAM into an open conformation with a ca. 11 Å wide and 22 Å deep channel [8, 9]. In the P450CAM open conformation, the F and G helices are displaced ca. 1 helical turn across the I helix so that the F/G domain moves away from the P450CAM  $\beta$ -sheet domain (Fig. 5) [8, 9]. The F/G loop and certain other residues along the E, F, and G helices function as hinges to facilitate this movement (Fig. 6) [9], while long side chains on the F, G, and I helices allow hydrogen bonding contacts between the F/G domain and the I helix [8]. The H helix and the N-terminus of the I helix move with the G helix so as to further maintain interhelical contacts.

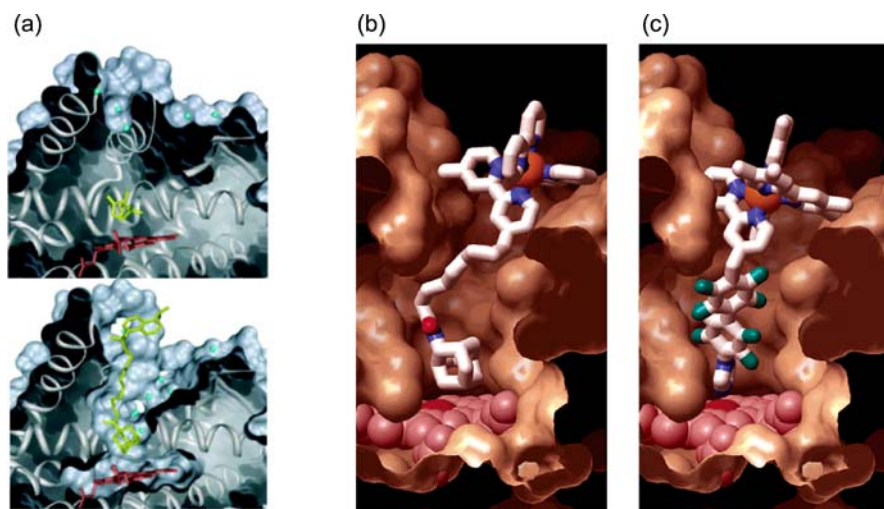


**Fig. 4** Cutaway views of the crystallographically determined structures of P450CAM wire complexes: (a) Comparison of the closed P450CAM conformation in its complex with camphor (*top*) and the open conformation adopted in its complex with D-8-Ad (*bottom*) (reproduced by permission from [9]). (b) Structure of the P450CAM:  $[\text{Ru} - \text{C}_9 - \text{Ad}]^{2+}$  complex compared with (c) a model of the P450CAM:  $[\text{tmRu} - \text{F}_8\text{bpy} - \text{Im}]^{2+}$  complex. Reproduced by permission from [33]

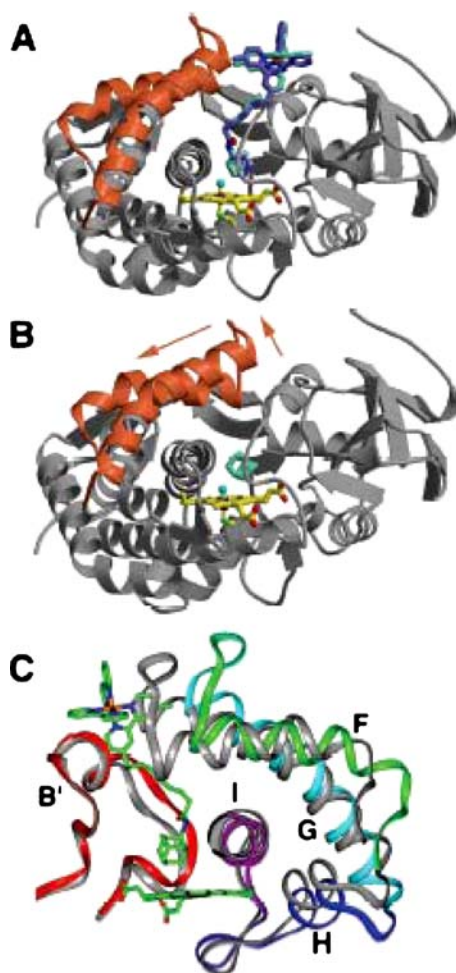


**Fig. 5** Comparison between the structure of P450CAM bound to **A**  $[\text{Ru}-\text{C}_9-\text{Ad}]^{2+}$  and **B** adamantane illustrating the displacement of the F/G subdomain across the I helix that occurs on formation of the P450CAM:  $[\text{Ru}-\text{C}_9-\text{Ad}]^{2+}$  complex. **C** Structure of the P450CAM:  $[\text{Ru}-\text{C}_9-\text{Ad}]^{2+}$  complex showing contacts between the F, G, I, and H helices. Reproduced with permission from [8]

Molecular wires with shorter tethers or more sterically demanding head groups are accommodated mainly by opening of the F/G subdomain, not by changes in substrate coordination at the active site. The extreme open conformation occurs in conjugates with  $[\text{Ru}-\text{C}_9-\text{Ad}]^{2+}$  [11] and  $[\text{Ru}-\text{F}_8\text{bpy}-\text{Ad}]^{2+}$  [8], which possess bulky  $[\text{Ru}(\text{bpy})_3]^{2+}$  head groups. Binding of the smaller D-4-Ad and D-8-Ad wires produces increasingly smaller conformational changes that involve the disruption of fewer interhelix interactions (Fig. 6) [9]. In particular, salt bridges and hydrogen bonding

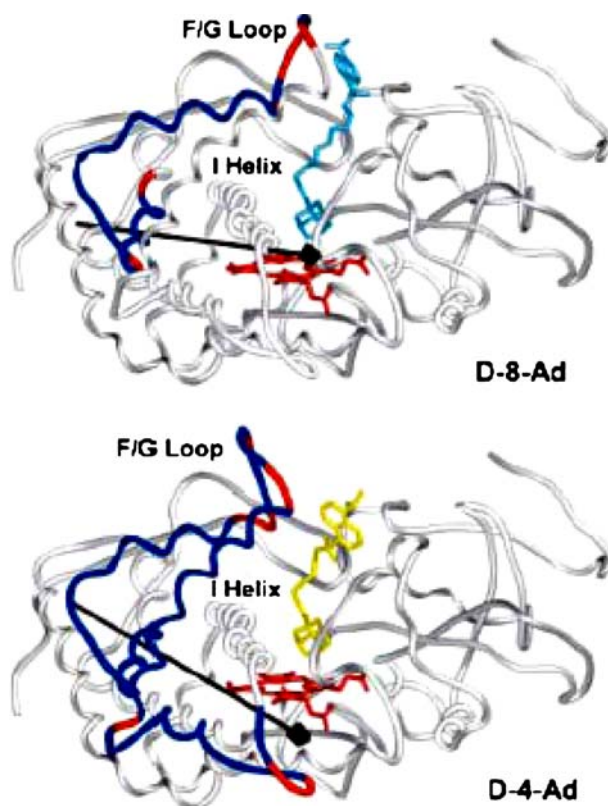


**Fig. 6** Molecular structures of the P450CAM: D-8-Ad (*top*) and P450CAM: D-4-Ad (*bottom*) complexes showing the specific domains that are significantly displaced on wire binding (*blue*) by rotational motion about hinge residues (*red*) that undergo large ( $\phi/\psi$ ) changes. The axis of the rotational motion is shown as a *black arrow*. Reproduced with permission from [9]

interactions between the F and I and B' and G helices are disrupted in the more open D-4-Ad complex, while only interactions between the F and I helices are broken in the D-8-Ad complex [9]. The overall effect of D-8-Ad binding is a more localized retraction of the F helix from the closed position, whereas D-4-Ad causes an additional retraction of the G helix. Essentially, these interactions permit the F/G subdomain to act as an adjustable clamp to hold the wire in place while excluding excess water from the active site [8].

The conformational movements associated with formation of open structures affect the positions of several catalytically important residues in the active site. The I helix bulge, which controls the water structure about the heme, and the catalytically relevant Asp<sup>251</sup> and Thr<sup>252</sup> residues are displaced into positions similar to those observed on dioxygen binding (Fig. 7) [9]. In

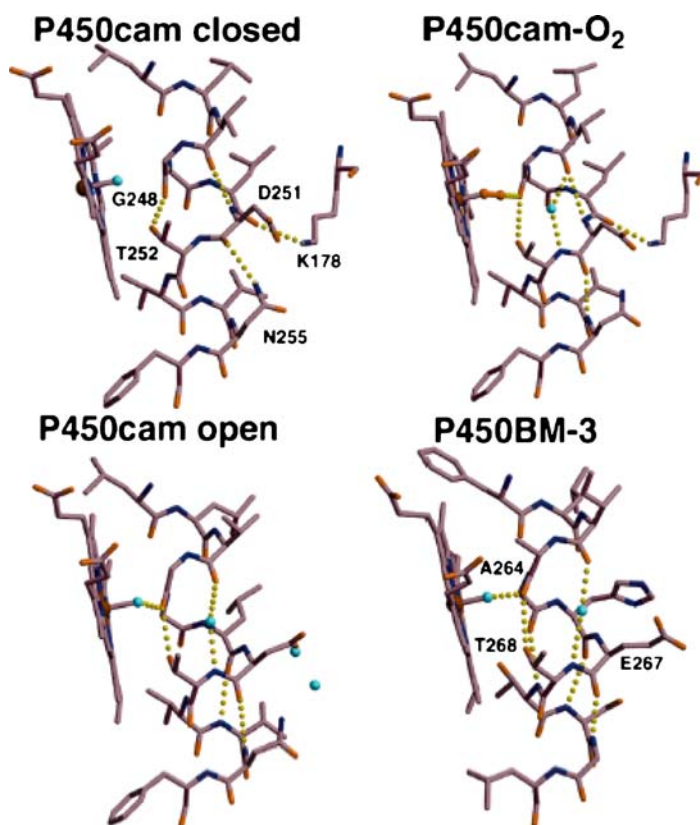


**Fig. 7** Comparison of the active-site structures of native (*closed*) P450CAM, P450CAM: O<sub>2</sub>, open P450CAM, and P450BM3. Reproduced with permission from [8]

particular, Asp<sup>251</sup>, which has been implicated in proton delivery to the active site, becomes hydrated on formation of the open conformation.

It is likely that these open conformations correspond to the structures of transient intermediates that are formed when substrates enter or products leave the active site [9]. The F/G loop occupies similar positions in other P450 isoforms, including substrate-free P450BM3 and P450NOR [41–43], and it is disordered in the crystal structures of P450terp and P4502C5 [44, 45]. The transient existence of open intermediates is supported by photoacoustic calorimetry [46, 47], cooperative substrate hydroxylation [48] and mutagenesis studies, [49] as well as computer simulations [50–52] with a variety of P450 isoforms.

Interestingly, P450:wire conjugates in the open conformation show catalytic activity. When P450:[Ru – C<sub>9</sub> – Ad]<sup>2+</sup> was treated with NADH in the presence of Pdx and Pdx reductase, the reductant was consumed at a rate of  $8 \pm 2$  mol/min/ $\mu$ mol P450, whereas product assays showed 10% formation of

the hydroxylated wire,  $[\text{Ru} - \text{C}_9 - \text{Ad} - \text{OH}]^{2+}$  [35]. Control experiments with 2-adamantylacetamide revealed a turnover rate of  $\sim 90 \pm 20 \text{ mol min}^{-1} \mu\text{mol P450}^{-1}$ . The lower rate observed for  $\text{P450}:[\text{Ru} - \text{C}_9 - \text{Ad}]^{2+}$  could be a consequence of conformational changes near  $\text{Asp}^{251}$  and  $\text{Thr}^{252}$  associated with  $[\text{Ru} - \text{C}_9 - \text{Ad}]^{2+}$  binding.

The crystallographic structures of wire:P450CAM complexes further underscore the importance of hydrophobic contacts for wire binding. The most striking results have been obtained for the complex with  $[\text{Ru} - \text{F}_8\text{bpy} - \text{Ad}]^{2+}$ , which possesses an electron-poor octafluorobiphenyl tether that is capable of forming strong parallel and perpendicular  $\pi$ -stacking interactions with electron-rich aromatic residues along the enzyme channel. As shown in Fig. 8, close contacts are made with  $\text{Tyr}^{29}$ ,  $\text{Phe}^{193}$ ,  $\text{Thr}^{87}$ , and  $\text{Tyr}^{96}$ . Of these,  $\text{Phe}^{193}$  is parallel to one of the octafluorobiphenyl rings with a 3.4 Å face-to-face distance, while  $\text{Phe}^{87}$  and  $\text{Tyr}^{96}$  are perpendicular to the biphenyl ring [8].

The results with alkyl-tethered wires further illuminate the wire:P450CAM interactions that can be exploited in inhibitor design. In these complexes, the hydrocarbon tether contacts hydrophobic residues along the active-site channel,  $\text{Ile}^{395}$ ,  $\text{Phe}^{193}$ ,  $\text{Phe}^{87}$ , and  $\text{Tyr}^{96}$ , many of which also are involved in binding the biphenyl moiety of  $[\text{Ru} - \text{F}_8\text{bpy} - \text{Ad}]^{2+}$  [8]. The flexible hydrocarbon tether permits the adamantyl moiety to adopt a favorable conformation in the active-site pocket, making extensive hydrophobic contacts with  $\text{Leu}^{244}$ ,  $\text{Thr}^{101}$ ,  $\text{Ile}^{395}$ ,  $\text{Val}^{295}$ ,  $\text{Thr}^{252}$ , and  $\text{Gly}^{248}$ . Complexes with hydrocarbon-tethered wires also make hydrogen bonding contacts between the adamantyl amide carbonyl and  $\text{Tyr}^{96}$  that are analogous to those observed between  $\text{Tyr}^{96}$  and the camphor ketone in the native enzyme [53]. In the  $[\text{Ru} - \text{C}_9 - \text{Ad}]^{2+}$  [11] and  $[\text{Ru} - \text{F}_8\text{bpy} - \text{Ad}]^{2+}$  [8] structures, the

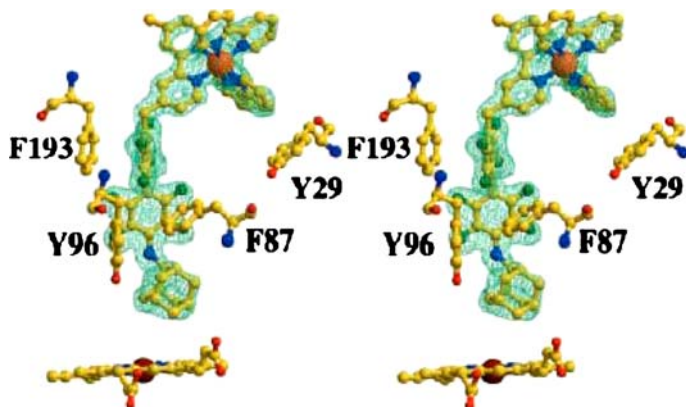


**Fig. 8** Structure of  $[\text{Ru} - \text{F}_8\text{bpy} - \text{Ad}]^{2+}$  bound to P450CAM showing interaction of the  $[\text{Ru}(\text{bpy})_3]^{2+}$  head group and octafluorobiphenyl tether with aromatic residues lining the active-site channel

[Ru(bpy)<sub>3</sub>]<sup>2+</sup> head groups of the  $\Lambda$  and  $\Delta$  enantiomers occupy different positions, making hydrophobic contacts with Tyr<sup>29</sup> and Pro<sup>187</sup>. These interactions at the mouth of the active-site channel contribute to substrate binding and serve to anchor the head group in place. Indeed, the hydrocarbon tether in the [Ru – F<sub>8</sub>bpy – Ad]<sup>2+</sup> complex is not fully extended and FET measurements (Table 1) indicate that the Ru-heme distance does not vary with tether length in other alkyl-tethered P450CAM:wire complexes.

Consistent with the above findings, multiple binding modes have been observed in the external portion of the D-8-Ad wire bound to P450CAM. The dansyl group is found in different conformations on the surface of the protein in two separate crystals of D-8-Ad bound to P450CAM, whereas the inner portions of the wire are bound identically (Fig. 9). Interestingly, the interactions of the dansyl groups with the protein are very similar in each of these conformations, owing to the rather symmetric disposition of Pro<sup>89</sup> on the B' helix and Pro<sup>187</sup> in the F/G loop.

Even after extensive structural characterization, one aspect of P450CAM binding to D-8-Ad remains puzzling. Addition of either D-8-Ad or D-4-Ad to P450CAM causes a partial spin-state shift (as judged by changes in the heme Soret absorbance) and efficient quenching of dansyl fluorescence (FET to the heme) [10]. Titration of camphor into samples of either complex causes a spin-state shift, consistent with binding of camphor at the enzyme active site. However, while camphor addition to the P450CAM:D-4-Ad complex

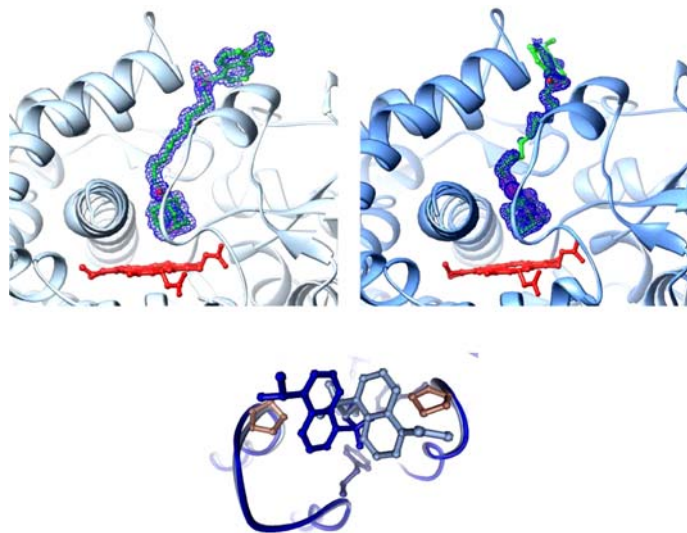


**Fig. 9** Crystal structures of two separate crystals of P450CAM bound to D-8-Ad at 1.45 Å (*left*) and 2.2 Å (*right*) resolution. In the higher resolution structure the dansyl group is found to make an interaction with Pro187 in the F/G loop while in the other crystal the dansyl is packed in a similar way against Pro89 of the B' helix

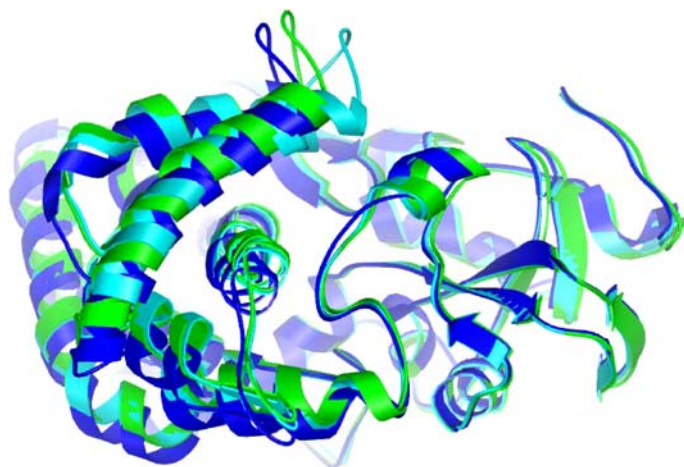


**Fig. 10** Comparison of the refined protein backbone ribbons for P450CAM complexed with D-8-Ad (*cyan*), D-4-Ad (*green*), and D-8-Ad with camphor (*blue*)

causes a recovery of fluorescence, indicating camphor induced release of the wire, no fluorescence recovery is observed when camphor is added to the P450CAM:D-8-Ad complex. This finding suggests that camphor binding to the protein does not lead to displacement of the D-8-Ad wire.

The 1.9 Å crystal structure of P450CAM in the presence of both D-8-Ad and camphor reveals that the F/G region is in a more open conformation than either D-8-Ad or D-4-Ad alone (Fig. 10). In addition, a segment of the B' helix is more disordered than in the absence of camphor and significant movement is seen in the I helix. Further, the wire electron density occupies the approximate location observed in the camphor-free P450CAM: wire structure, but it is not as well resolved. Unfortunately, because of the possible presence of D-8-Ad and/or camphor in the substrate channel, the camphor position in this structure could not be unambiguously defined, although solution measurements suggest that camphor binds at the active site, but does not completely displace the D-8-Ad wire from the channel. Apparently, P450CAM can simultaneously bind wire and camphor by further opening of the flexible active-site channel.

### 2.3 Sensing

The photophysical and selective binding properties of molecular wires have been exploited to develop highly sensitive and selective fluorescent probes of active sites (Fig. 11). Initial work using alkyl-tethered  $[\text{Ru}(\text{bpy})_3]^{2+}$ -based wires established the feasibility of selectively detecting P450CAM at sub-micromolar concentrations by monitoring the decrease in emission life-

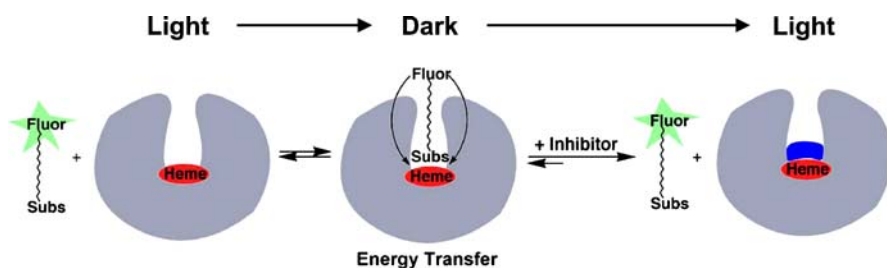


**Fig. 11** Principle of FET detection with P450: wires showing the “light to dark” method for enzyme detection and “dark to light” method for inhibitor screening

time on binding [11]. These assays were found to be highly specific for P450CAM: no change in wire lifetime was observed for other heme proteins, including yeast cytochrome c, horse skeletal muscle myoglobin, bovine lipase, cytochrome b<sub>5</sub>, bovine liver catalase, recombinant yeast cytochrome c peroxidase, and horseradish peroxidase [11]. Based on these results, wires consisting of a dansyl fluorophore tethered to an adamantyl substrate via an  $\alpha, \omega$ -diaminoalkane tether were developed as highly sensitive optical probes for inhibitor screening [10]. These wires bind P450CAM tightly ( $K_d \sim 0.02\text{--}0.83 \mu\text{M}$ ) and exhibit greatly decreased fluorescence in the presence of P450CAM which, in the case of D-4-Ad, can be restored by competition with other substrates, such as camphor (Fig. 12).

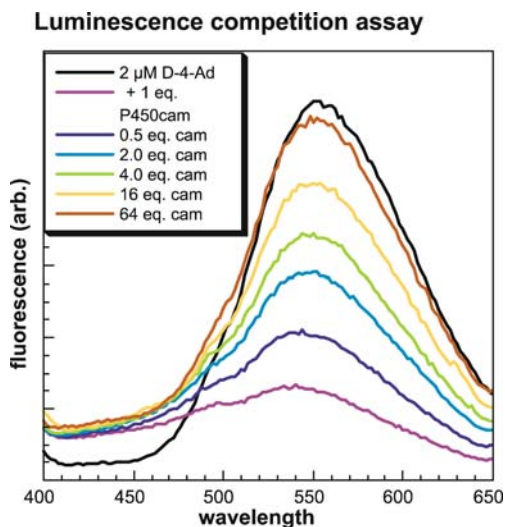


**Fig. 12** Fluorescence spectra of D-4-Ad showing the loss of emission on addition of one equivalent of P450CAM and recovery of emission on addition of camphor

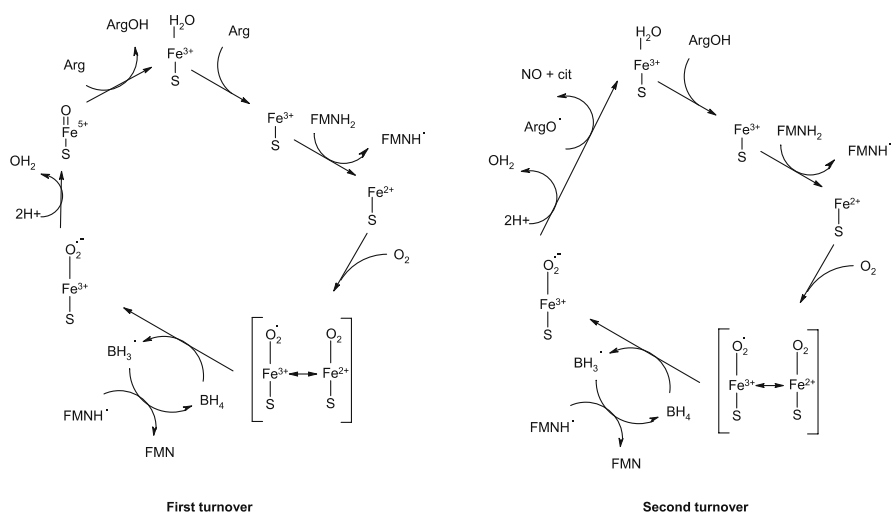
### 3 Molecular Wires for Inducible Nitric Oxide Synthase

NOS is an important signaling enzyme that synthesizes L-citrulline and nitric oxide (NO) from L-arginine and  $O_2$  via two turnovers in a P450-like catalytic cycle (Scheme 2). NOS participates in physiological processes such as neurotransmission, vasodilation, and immune response [54, 55]. Improper regulation of NO production can lead to diseases such as septic shock, heart disease, arthritis, and diabetes.

Three isoforms of NOS are produced in mammalian cells: neuronal (nNOS), endothelial (eNOS), and inducible (iNOS) [55]. All NOS isoforms exist as homodimers with a C-terminal FMN-FAD fused reductase domain, an N-terminal oxygenase domain, and a calmodulin binding sequence at the interface of the two domains. The NOS catalytic mechanism is complicated and requires  $O_2$ , NADPH, FMN, FAD,  $Ca^{2+}$ , calmodulin, tetrahydrobiopterin ( $BH_4$ ), and heme to effect the five-electron oxidation of L-arginine to L-citrulline and NO. Consumed in this process are 1.5 equivalents of NADPH and 2 equivalents of  $O_2$ .

The differences in structures and redox partners between the two classes of P450 and NOS enzymes give rise to differences in reduction potentials and electron transfer mechanisms. The fusion of the oxygenase domain to its di-flavin reductase domain facilitates ET (of relevance here is that P450 BM3 has the highest mono-oxygenase activity of all P450s [56]).

We have employed molecular wire complexes to probe the ET mechanisms of iNOS. Although we have yet to definitively characterize an iNOS:wire con-



**Scheme 2** Proposed NOS catalytic cycle

jugate by X-ray diffraction, our work has elucidated the factors that govern substrate binding in the iNOS active-site channel and on the enzyme surface. Furthermore, comparison of these results with those obtained with P450CAM has shed light on the energetics of wire-enzyme complexation.

### 3.1 Binding

Given the mechanistic similarities between P450 and NOS, our initial work with iNOS focused on molecular wires that are structurally similar to those employed with P450CAM [12, 57]. In addition, most experiments involved the oxygenase domain of inducible NOS (iNOS<sub>oxy</sub>), with N-terminal truncations at amino acid residue 65 (NOS  $\Delta$ 65) and residue 114 (NOS  $\Delta$ 114). Structural differences between the two truncated iNOS species play an important role in wire inhibition and binding: NOS  $\Delta$ 114 exists mainly in monomeric form, whereas NOS  $\Delta$ 65 exists in equilibrium between monomeric and dimeric states and forms tight dimers in the presence of L-arginine and tetrahydrobiopterin (BH<sub>4</sub>) [58]. The NOS monomer has an exposed active site, while NOS dimer has a more constricted access channel.

Molecular wires with [Ru(bpy)<sub>3</sub>]<sup>2+</sup> head groups that bind  $\Delta$ 65 and  $\Delta$ 114 iNOS<sub>oxy</sub> are shown in Fig. 13. Most of these wires are extremely hydropho-

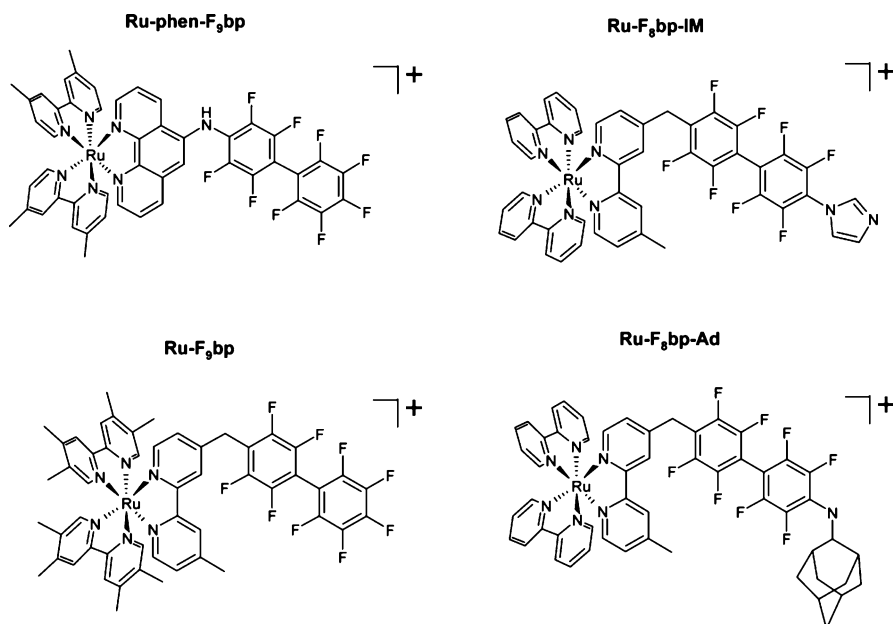


**Fig. 13** Ruthenium wires that bind iNOS<sub>oxy</sub>

bic, owing in part to a decafluorobiphenyl tether. The hydrophobicity of these complexes is further increased by addition of adamantyl groups to the decafluorobiphenyl ring and/or the use of 4,4',5,5'-tetramethylbipyridine co-ligands at the ruthenium center.

Wire binding to iNOS was quantified in work involving both time-resolved and steady-state emission experiments. The results confirm that iNOS:wire conjugates have nanomolar or low micromolar dissociation constants (Table 2) and that the wire binding interactions are not significantly affected by co-binding of L-arginine and BH<sub>4</sub>. In each truncated form ( $\Delta 65$  and  $\Delta 114$  iNOS<sub>oxy</sub>), there is substantial energy transfer quenching of the Ru(II) MLCT excited state. FET kinetics indicate that the wires bind the protein such that the head group is positioned within ca. 18–21 Å of the heme active site. Our analyses of the absorption spectra of iNOS:wire conjugates suggest that the steric bulk of the substrate group and the tether length govern the mode of wire binding. Interestingly, only the weakest binding wire, [Ru – F<sub>8</sub>bp – Im]<sup>2+</sup>, which ligates the heme Fe, displaces L-arginine from the active site.

Based on modeling work, it is not likely that [Ru – F<sub>9</sub>bp]<sup>2+</sup> and [Ru – phen – F<sub>9</sub>bp]<sup>2+</sup> will fit in the active-site channel of  $\Delta 65$ , owing to the bulk of the [Ru(bpy)<sub>3</sub>]<sup>2+</sup> head group (Fig. 14b) [13, 36, 59]. Examination of the FET-determined distances suggests that these wires bind either to the iNOS surface or the mouth of active-site channel but are too short to reach the deeply buried active site. Modeling indicates that [Ru – F<sub>8</sub>bp – Ad]<sup>2+</sup> cannot reach the active sites of  $\Delta 65$  or  $\Delta 114$  iNOS<sub>oxy</sub>, owing to the steric bulk of the adamantyl group, although [Ru – F<sub>8</sub>bp – Im]<sup>2+</sup> should be able to bind to the more open active site of monomeric  $\Delta 114$  iNOS<sub>oxy</sub> (Fig. 14). In addition, the presence of excess electron density at a concave hydrophobic patch on the oxygenase-reductase interface surface in a partial crystal structure of iNOS:[Ru – F<sub>8</sub>bp – Ad]<sup>2+</sup> is consistent with wire binding at this surface position [36, 59].

Our results confirm that the iNOS active-site channel is considerably less plastic than that of P450CAM. In addition, they suggest that ruthenium wires could inhibit iNOS activity by blocking electron transfer between the reductase and oxygenase domains.

**Table 2** iNOS:wire conjugates

Wire	$\Delta 114$ (K <sub>d</sub> , $\mu$ M)	$\Delta 65$ (K <sub>d</sub> , $\mu$ M)	$\Delta 65 + \text{arg} + \text{BH}_4$ (K <sub>d</sub> , $\mu$ M)	Refs.
[Ru – phen – F <sub>9</sub> bp] <sup>2+</sup>	–	0.5 ± 0.15	–	[59]
[Ru – F <sub>9</sub> bp] <sup>2+</sup>	0.71 ± 0.09	0.54 ± 0.04	1.7 ± 0.4	[57]
[Ru – F <sub>8</sub> bp – Im] <sup>2+</sup>	7.1 ± 0.4	6.5 ± 2.4	7.2 ± 3.4	[57]
[Ru – F <sub>8</sub> bp – Ad] <sup>2+</sup>	0.88 ± 0.15	0.58 ± 0.16	0.89 ± 0.15	[57]

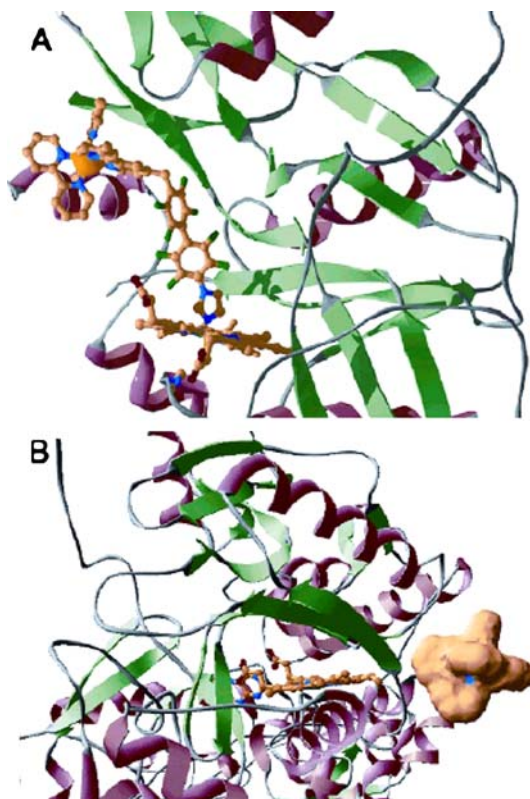


**Fig. 14** **A** Model of  $[\text{Ru}-\text{F}_8\text{bp}-\text{Im}]^{2+}$  bound to the exposed heme of NOS  $\Delta 114$ . **B** Model of  $[\text{Ru}(\text{bpy})_3]^{2+}$  docked at the proposed oxygenase-reductase interface. Reproduced from [13]

In related work, we found that use of a smaller head group,  $[\text{Re}(\text{CO})_3(\text{bpy})(\text{Im})]^+$  [60], promotes wire binding to the deeply buried iNOS active site. The four rhenium wires that have been investigated most extensively as probes of iNOS<sub>oxy</sub> are shown in Fig. 15 [12, 36].

All four wires bind in the active-site channel of the enzyme with low micromolar or nanomolar dissociation constants (Table 3). Analysis of the heme Soret suggests that the active-site structure converts from six-coordinate low-spin to five-coordinate high-spin in complexes with  $[\text{Re}-\text{Im}-\text{F}_9\text{bp}]^+$  and  $[\text{Re}-\text{Im}-\text{C}_3-\text{F}_9\text{bp}]^+$ , indicative of water displacement from the heme region. The two imidazole-terminated wires,  $[\text{Re}-\text{Im}-\text{F}_8\text{bp}-\text{Im}]^+$  and  $[\text{Re}-\text{Im}-\text{C}_3-\text{F}_8\text{bp}-\text{Im}]^+$ , both displace water and ligate the heme, as judged by observation of the characteristic “low-spin shift” of the heme Soret band.

In summary, our results show that wires with sterically demanding  $[\text{Ru}(\text{bpy})_3]^{2+}$  head groups bind with low-micromolar to nanomolar disso-

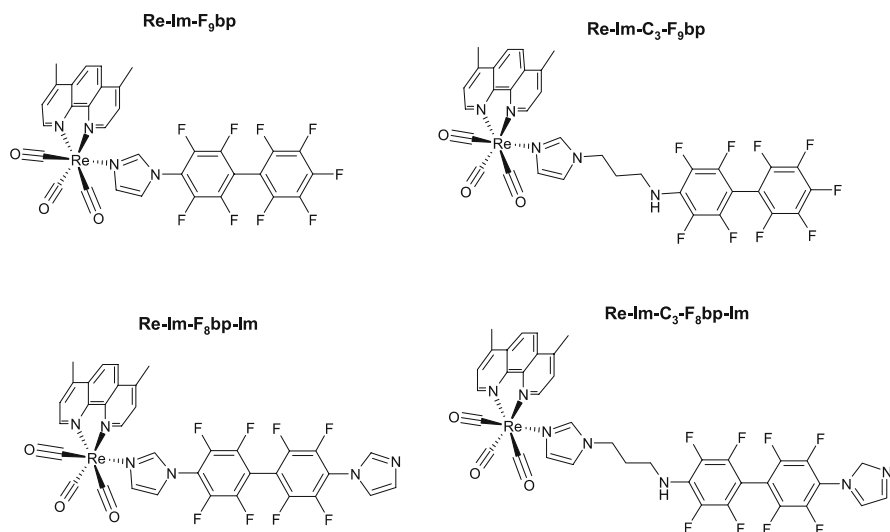


**Fig. 15** Rhenium wires that bind iNOS<sub>oxy</sub>

**Table 3** Dissociation constants for Re wires with  $\Delta 65$  iNOS<sub>oxy</sub>

Wire	$\Delta 65$ , $K_d$ ( $\mu\text{M}$ )	Wire	$\Delta 65$ , $K_d$ ( $\mu\text{M}$ )
$[\text{Re} - \text{Im} - \text{F}_9\text{bp}]^+$	1.4	$[\text{Re} - \text{Im} - \text{C}_3 - \text{F}_9\text{bp}]^+$	< 10
$[\text{Re} - \text{Im} - \text{F}_8\text{bp} - \text{Im}]^+$	0.13	$[\text{Re} - \text{Im} - \text{C}_3 - \text{F}_8\text{bp} - \text{Im}]^+$	< 10

ciation constants to the iNOS surface, presumably at the oxygenase and reductase interface, whereas wires with  $[\text{Re}(\text{CO})_3(\text{bpy})(\text{Im})]^+$  head groups bind in the active-site channel with similar affinities [13]. When compared to the remarkable indifference of P450CAM:wire stability to the steric bulk of the head group, these results underscore the importance of protein plasticity in wire binding. Additionally, the remarkable disparity in structure between the rhenium channel-binding wires and the natural substrate, L-arginine, suggests that binding is driven principally by hydrophobic interactions with active-site channel residues [13].

### 3.2 Sensing

While we have not aggressively attempted to develop fluorescent sensors for iNOS, FET and ET quenching by the heme of the MLCT excited states of  $[\text{Ru}(\text{bpy})_3]^{2+}$  and  $[\text{Re}(\text{CO})_3(\text{bpy})(\text{Im})]^+$  head groups enable the wires shown in Fig. 13 and 15 to function as effective “light-to-dark” probes of the en-

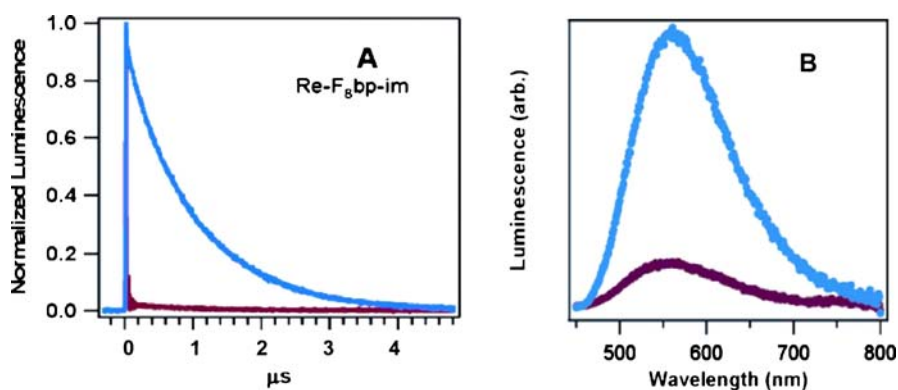


**Fig. 16** **A** Time-resolved and **B** steady-state luminescence of  $[\text{Re} - \text{Im} - \text{F}_8\text{bp} - \text{Im}]^+$  in the presence of  $\text{iNOS}_{\text{oxy}}$ . Reproduced from [12]

zyme. The most promising of these are the rhenium-based wires, whose MLCT excited states are strongly quenched by ultrafast ET to the iNOS heme (Fig. 16) [12, 13, 36]. Given the ability of iNOS to form wire complexes with nanomolar dissociation constants, it should be possible to develop extremely sensitive dansyl or fluorescein-based FET wire sensors for the enzyme.

## 4

### Conclusions

Photoactive wire probes are powerful tools for studying protein mechanism and function, enabling rapid photogeneration of reactive enzyme redox states and systematic study of the structural factors that govern substrate binding and promiscuity. Additionally, they show promise as high affinity and isoform specific fluorescent protein sensors, electrochemical probes, and crystallographic tools for studying the open states of enzymes.

Through an understanding of the structure of the native enzyme, we have designed selective probes that successfully target and interrogate P450CAM and iNOS. In turn, structural studies of wire-enzyme complexes have provided a wealth of information. They have elucidated the chemical features that dictate the binding mode and affinity for the enzyme, and have revealed the conformational flexibility of the protein, trapping structures that mimic transient intermediates associated with substrate binding through catalysis to product release.

Working at the interface of chemistry and biology, we are exploiting techniques at the two extremes of the time scale for protein research: ultrafast photoreduction of the enzyme by these metal-diimine wires affords access to catalytic intermediates on the time scale of electron transfer, while X-ray crys-

tallography of enzyme:wire conjugates provides complementary snapshots of *static* structures. The goal of fast reduction of a deeply buried heme via a wire has been accomplished with iNOS, while detailed structural analyses with a variety of wires have provided new information about the conformational states of P450CAM, and has offered clues for creating inhibitors that take advantage of its structural flexibility.

**Acknowledgements** Figure 11 was adopted from a version prepared by Alex Dunn. We thank him and others in the Caltech molecular wires group (Ivan Dmochowski, Jon Wilker, Corinna Hess, Wendy Belliston-Bittner, Nick Halpern-Manners) for contributions that are summarized in this chapter. Our work is supported by NIH, NSF, the Ellison Medical Foundation Senior Scholar Award in Aging (to HBG), and the Arnold and Mabel Beckman Foundation.

## References

1. Roberts GA, Grogan G, Greter A, Flitsch SL, Turner NJ (2002) *J Bacteriol* 184:3898
2. Boddupalli SS, Oster T, Estabrook RW, Peterson JA (1992) *J Biol Chem* 267:10375
3. Warman AJ, Roitel O, Neeli R, Girvan HM, Seward HE, Murray SA, McLean KJ, Joyce MG, Toogood H, Holt RA, Leys D, Scrutton NS, Munro AW (2005) *Biochem Soc Trans* 33:747
4. Fuziwara S, Sagami I, Rozhkova E, Craig D, Noble MA, Munro AW, Chapman SK, Shimizu T (2002) *J Inorg Biochem* 91:515
5. Low DW, Winkler JR, Gray HB (1996) *J Am Chem Soc* 118:117
6. Wilker JJ, Dmochowski IJ, Dawson JH, Winkler JR, Gray HB (1999) *Angew Chem Int Ed* 38:90
7. Dmochowski IJ, Dunn AR, Wilker JJ, Crane BR, Green MT, Dawson JH, Sligar SG, Winkler JR, Gray HB (2002) *Method Enzymol* 357:120
8. Dunn AR, Dmochowski IJ, Bilwes AM, Gray HB, Crane BR (2001) *Proc Natl Acad Sci USA* 98:12420 x
9. Hays A-MA, Dunn AR, Chiu R, Gray HB, Stout CD, Goodin DB (2004) *J Mol Biol* 344:455
10. Dunn AR, Hays A-MA, Goodin DB, Stout CD, Chiu R, Winkler JR, Gray HB (2002) *J Am Chem Soc* 124:10254
11. Dmochowski IJ, Crane BR, Wilker JJ, Winkler JR, Gray HB (1999) *Proc Natl Acad Sci USA* 96:12987
12. Belliston-Bittner W, Dunn AR, Nguyen YHL, Stuehr DJ, Winkler JR, Gray HB (2005) *J Am Chem Soc* 127:15907
13. Dunn AR, Belliston-Bittner W, Winkler JR, Getzoff ED, Stuehr DJ, Gray HB (2005) *J Am Chem Soc* 127:5169
14. Hess CR, Juda GA, Dooley DM, Amii RN, Hill MG, Winkler JR, Gray HB (2003) *J Am Chem Soc* 125(24):7156
15. Contakes SM, Juda GA, Langley DB, Halpern-Manners NW, Duff AP, Dunn AR, Gray HB, Dooley DM, Guss JM, Freeman HC (2005) *Proc Natl Acad Sci USA* 102:13451
16. Gray HB, Dunn AR, Belliston W, Leigh BS, Contakes SM, Winkler JR (2003) 225th ACS National Meeting, New Orleans, LA, USA
17. Kenyon V, Chorny I, Carvaja SW, Holman TR, Jacobson MP (2006) *J Med Chem* 49:1356

18. Lewis DFV (2001) *Guide to Cytochromes P450: Structure and Function*. CRC Press, New York
19. Ortiz de Montellano PR (1995) *Cytochrome P450: Structure, Mechanism, and Biochemistry*. Plenum Press, New York, p 652
20. Phillips IR, Shephard EA (1998) *Methods in Molecular Biology*, vol 107. Humana Press, Totowa, p 482
21. Sono M, Roach MP, Coulter ED, Dawson JH (1996) *Chem Rev* 96:2842
22. Guengerich FP (2003) *Mol Interv* 3:194
23. Glieder A, Farinas ET, Arnold FH (2002) *Nat Biotechnol* 20:1135
24. Joseph S, Rusling JF, Lvov YM, Friedberg T, Fuhr U (2003) *Biochem Pharmacol* 65:1817
25. Davydov R, Markris TM, Kofman V, Werst DE, Sligar SG, Hoffman BM (2001) *J Am Chem Soc* 123:1403
26. Egawa T, Shimada H, Ishimura Y (1994) *Biochem Biophys Res Commun* 201:1464
27. Schlichting I, Berendzen J, Chu K, Stock AM, Maves SA, Benson DE, Sweet RM, Ringe D, Petsko GA, Sligar SG (2000) *Science* 287:1615
28. Glascock MC, Ballou DP, Dawson JH (2005) *J Biol Chem* 280:42134
29. Udit A, Contakes SM, Gray HB (2007) *Met Ions Life Sci* 3:in press
30. Udit A (2005) P450 BM3 electrochemistry and electrocatalysis. PhD, California Institute of Technology
31. Noble M, Miles C, Chapman S, Lysek D, Mackay A, Reid G, Hanzlik R, Munro A (1999) *Biochem J* 339:371
32. Sevrioukova IF, Li H, Zhang H, Petersson JA, Poulos TL (1999) *Proc Natl Acad Sci USA* 96:1863
33. Dunn AR, Dmochowski IJ, Winkler JR, Gray HB (2003) *J Am Chem Soc* 125:12450
34. Dunn AR (2003) Sensitizer-linked substrates as probes of heme enzyme structure and catalysis. PhD, California Institute of Technology
35. Dmochowski IJ (2000) Probing Cytochrome P450 with Sensitizer-linked Substrates. Ph.D., California Institute of Technology
36. Belliston Bittner W (2005) Ultrafast Photoreduction of Nitric Oxide Synthase by Electron Tunneling Wires. PhD, California Institute of Technology
37. Lipscomb JD (1980) *Biochemistry* 19:3590
38. Poulos TL, Howard AJ (1987) *Biochemistry* 26:8165
39. Dmochowski IJ, Winkler JR, Gray HB (2000) *J Inorg Biochem* 81:221
40. Raag R, Poulos TL (1991) *Biochemistry* 30:2674
41. Ravichandran KG, Boddupalli SS, Hasemann CA, Peterson JA, Deisenhofer J (1993) *Science* 261:731
42. Li H, Poulos TL (1997) *Nat Struct Biol* 4:140
43. Park SY, Shimizu H, Adachi S, Nakagawa A, Tanaka I, Nakahara K, Shoun H, Obayashi E, Nakamura H, Iizuka T, Shiro Y (1997) *Nat Struct Biol* 4:827
44. Hasemann CA, Kurumbail RG, Boddupalli SS, Peterson JA, Deisenhofer J (1995) *Structure* 2:41
45. Williams PA, Cosme J, Sridhar V, Johnson EF, McRee DE (2000) *Molec Cell* 5:121
46. DiPrimo C, Hoa GHB, Deprez E, Douzou P, Sligar SG (1993) *Biochemistry* 32:3671
47. DiPrimo C, Deprez E, Sligar SG, Hoa GHB (1997) *Biochemistry* 36:112
48. Ueng Y-F, Kuwabara T, Chun Y-J, Guengerich FP (1997) *Biochemistry* 36:371
49. Podust LM, Poulos TL, Waterman MR (2001) *Proc Natl Acad Sci USA* 98:3068
50. Paulsen MD, Ornstein RL (1995) *Proteins* 21:237
51. Poulos TL (1995) *Curr Opin Struct Biol* 5:767
52. Ludemann SK, Lounnas V, Wade RC (2000) *J Mol Biol* 303:797

53. Poulos TL, Finzel BC, Gunsalus IC, Wagner GC, Kraut J (1985) *J Biol Chem* 260:16122
54. Marletta MA, Hurshman AR, Rusche KM (1998) *Curr Opin Chem Biol* 2:656
55. Stuehr DJ (1999) *Biochim Biophys Acta-Bioenerget* 1411:217
56. Daff S, Chapman S, Turner K, Holt R, Govindaraj S, Poulos T, Munro A (1997) *Biochemistry* 36:13816
57. Dunn AR, Belliston-Bittner W, Winkler JR, Getzoff ED, Stuehr DJ, Gray HB (2005) *J Am Chem Soc* 127:5169
58. Ghosh DK, Wu CQ, Pitters E, Moloney M, Werner ER, Mayer B, Stuehr DJ (1997) *Biochemistry* 36:10609
59. Nguyen YHL (2006) Wiring inducible nitric oxide synthase. PhD, California Institute of Technology
60. Gerstein M (1992) *Acta Cryst Sec A* 48:271